Available online at www.sciencedirect.com
SCIENCE DIRECT®
Journal of Sound and Vibration 279 (2005) 581–600
JOURNAL OF SOUND AND VIBRATION
www.elsevier.com/locate/jsvi

Purification and feature extraction of shaft orbits for diagnosing large rotating machinery

D.F. Shi[a,*], W.J. Wang[b], P.J. Unsworth[b], L.S. Qu[c]

[a] *Institute of Vibration Engineering Research, Nanjing University of Aeronautics and Astronautics, PR China*
[b] *School of Engineering & Information Technology, University of Sussex, Brighton BN1 9QT, UK*
[c] *Research Institute of Diagnostics & Cybernetics, Xian Jiaotong University, Xian 710049, PR China*

Received 13 January 2003; accepted 11 November 2003

Abstract

Vibration-based diagnosis has been employed as a powerful tool in maintaining the operating efficiency and safety for large rotating machinery. However, due to some inherent shortages, it is not accurate enough to extract the features of malfunctions by using traditional vibration signal processing techniques. In this paper, a high-resolution spectrum is firstly proposed to calculate the amplitude, frequency and phase details of sinusoidal harmonic and sub-harmonic vibration in large rotating machinery. Secondly, on the basis of a high-resolution spectrum, a purified shaft orbit is reconstructed to remove the interference terms. The moment and curve features, which are invariant to translation, scaling and rotation of the shaft orbit, are introduced to extract the features from the purified vibration orbit. This novel scheme is shown to be very effective and reliable in diagnosing several types of malfunctions in gas turbines and compressors under operating conditions as well as in the run-up stages.

1. Introduction

Large rotating machinery, such as gas turbines and centrifugal compressors, is crucial equipment in oil refineries, power plants, and chemical engineering plants. Competitiveness in the world market encourages such plants to reduce production losses and enhance efficiency and longevity in manufacturing processes. Vibration monitoring as part of the preventive maintenance programme has been widely employed to guarantee safety and reliability in manufacturing processes, and has proved to be highly cost effective [1,2]. In general, the vibration signals contain

*Corresponding author. Present address: School of Engineering, University of Manchester, Simon Building, Oxford Road, Manchester M13 9PL, UK. Tel.: +44-161-275-4453; fax: +44-161-275-4444.
E-mail address: dongfeng.shi@man.ac.uk (D.F. Shi).

0022-460X/$ - see front matter © 2004 Elsevier Ltd. All rights reserved.
doi:10.1016/j.jsv.2003.11.036

the symptoms of malfunctions and can be collected by two mutually perpendicular displacement sensors mounted on a bearing support. Furthermore, the received signals are pre-processed in order to suppress high frequency noise and direct current offset, then analogue-to-digital (A/D) converted and combined to construct a shaft orbit diagram. Finally, if the signals are fast Fourier transformed (FFT), the spectra revealing their composition in the frequency domain can be obtained [3].

Along with the development of signal processing and pattern recognition techniques, the vibration signal-based diagnosis for rotating machinery has attracted more and more attention. Some signal processing tools such as auto-spectrum, cross-spectrum, cespectrum and higher order spectrum based on FFT are introduced to diagnose the faults in rotating machinery [4–8]. Downham [4] made a comprehensive study of in malfunction diagnosis in rotating machinery by vibration analysis. Various faults which occurred in practice, such as whirl, turbine blade failure, and gear or bearing wear, were fully investigated. Muszynska [5, 6] extracted several specific features of malfunctions through rotor-bearing dynamics models. These malfunctions included unbalance, excessive radial load, rotor-to-stator rubbing, fluid excitation, part loosening and rotor cracking. Zheng and Wang [7] developed a new cepstral analysis technique to extract the multiple transient components from rotor vibration signals dominated by harmonic components. Some fault-related transient excitations, such as rubbing between the stator and rotor, have been diagnosed effectively using the above technique. In addition, some advanced time–frequency analysis tools, such as short time Fourier transform, Wigner distribution and wavelet transform have been introduced to analyze the non-stationary vibration behaviours of large rotating machinery [8–11]. In the field of fault feature extraction, Qu and Shen [12] introduced an information entropy theory to evaluate the complexity of the vibration orbit in rotating machinery. This method can be used to monitor the variation in vibration behaviour. However, it provides little information for pinpointing more details of the faults. Peng et al. [13] proposed a wavelet-based approach to extract the fault features from the vibration orbit, which has proved effective to diagnose up to four types of faults in rotating machinery, i.e. rotor unbalance, coupling misalignment, oil whip and rubbing.

On account of some inherent drawbacks, some signal processing techniques, such as FFT spectrum and original orbits cannot be used to extract reliably diagnostic features in practice. Firstly, the amplitude spectrum and phase spectrum can be obtained through FFT of the vibration signal. Unfortunately, the latter is always overlooked in application. If the phase information in vibration analysis is ignored, considerable information about rotor behaviours will be lost. Same amplitude spectra with different phases may correspond to completely different signals in time domain. Hence, a total adoption of amplitude, frequency and phase information is desirable to reveal comprehensively the characteristics of the vibration signal in the frequency domain. Secondly, the traditional spectral analysis method is unable to express the relationship between the horizontal and vertical vibration in a bearing. On the other hand, using the information fusion [14] of two mutually perpendicular signals one can discover the actual vibration behaviours of the rotor system. Since traditional feature extraction approaches have no way of correlating the internal temporal and spatial features of the faults, so the real machinery faults cannot be pinpointed. Thirdly, the traditional extracted features, such as peak-to-peak and root-mean-square, are concentrated on amplitude change caused by malfunctions, and have no way of evaluating the shape characteristics of the vibration orbit. If taking only amplitude-related

features into account, it is not reliable for detecting faults with relatively lower vibration energy at the early stage and will probably lead to serious misjudgment. Finally, in addition to the specific features of malfunction, the original vibration orbit contains plenty of interference components and noise. It is not feasible to diagnose the malfunctions by using the original orbit directly. Obviously, an efficient tool is required to extract definitive features of malfunction from the original orbit, which is always obscured by the interference terms and noise.

This paper aims at overcoming the shortcomings in traditional signal processing and feature extraction techniques, and provides a novel scheme based on multi-sensor fusion to purify and extract features from the vibration orbit for diagnosing the faults in rotating machinery. The paper is organized as follows. Section 2 introduces a new vibration orbit purification technique based on a high-resolution spectrum to calculate the frequency, phase and amplitude of harmonic and sub-harmonic components in the vibration signal. In Section 3, the moment and curve features, which are invariant to translation, scaling and rotation of the shaft orbit, are proposed to extract the features. The applications in diagnosis for industrial turbines and compressors in operational conditions as well as during the run-up stages are investigated in Section 4. Conclusions and recommendations are envisaged in the last section.

2. Purification of shaft orbits

2.1. Vibration characteristics of rotating machinery

Machine vibration contains the symptoms of malfunction and is related to change of input force or dynamic stiffness. Owing to the failure of component, the abnormal vibration can be generated from the rotor, pedestals, fluid and pipe system. According to the characteristics of vibration frequency, the faults can be classified as the harmonic-related fault, whose vibration energy concentrates in the harmonics of the synchronous frequency of the shaft, and sub-harmonic-related fault, whose vibration frequency is lower than the synchronous frequency. In general, the shaft vibrational displacements of rotating machinery in x and y directions can be expressed as

$$\begin{aligned} x(t) &= \sum_{i=1} A_i \sin(i2\pi f_0 t + \alpha_i) + \sum_{k=1} C_k \sin(\tau_k 2\pi f_0 t + \theta_k) + O_x(t), \\ y(t) &= \sum_{i=1} B_i \sin(i2\pi f_0 t + \beta_i) + \sum_{k=1} D_k \sin(\tau_k 2\pi f_0 t + \phi_k) + O_y(t), \end{aligned} \tag{1}$$

where i is the order of the harmonic vibration, f_0 is the synchronous rotating frequency; A_i, B_i are the ith harmonic vibration amplitude in horizontal and vertical directions, respectively; α_i, β_i are the initial phase of the ith harmonic vibration in the horizontal and vertical directions, respectively; τ_k is the coefficient of sub-harmonic vibration and less than 1; C_k, D_k are the sub-harmonic vibration amplitude in the horizontal and vertical directions, θ_k, ϕ_k are the kth initial phase of the sub-harmonic vibration in the horizontal and vertical directions, respectively; O_x O_y are the non-white-noise components and the frequency distribution is always lower than the synchronous rotating frequency.

If the machinery is fault-free except for rotor unbalance, the vibration will contain only the synchronous component. However, if some faults, such as a crack, coupling misalignment, on rubbing, occur in the machine, the sinusoidal vibration harmonic components will appear. If some other faults, such as oil whip, rotating stall, part loosening, seal wear and fluid excitation, occur in the machine, the vibration energy will be distributed in a low-frequency band (always lower than synchronous frequency) as a form of the sub-harmonic or non-white noise. In order to effectively extract the features of harmonic or sub-harmonic component-related faults, a reliable method is required to calculate the precise amplitude, frequency and phase for the above sinusoidal components.

2.2. Finding vibration parameters from high-resolution spectrum

Fourier transform is a powerful signal processing tool and can be used to analyze the composition of sinusoidal vibration signals of rotating machinery. Unfortunately, due to signal truncation in the time domain, leakage effects will more or less appear in discrete Fourier spectra despite the use of any type of window function [15]. In addition, an FFT spectrum is the result of continuous spectrum sampled with a frequency interval (Δf). In general, the exact location of a spectrum line may not be located in the centre of the main-lobe, and the estimated frequency, amplitude and phase of the vibration component are not accurate. This is the so-called comb-effect as illustrated in Figs. 1 and 2. Only if the sampling frequency is an integral multiple of the frequency of sinusoidal signal, the estimated frequency will be located in the centre of the main-lobe and equal to real frequency. Otherwise, this comb-effect result in an estimation error in frequency, amplitude and phase of a sinusoidal signal. If only a synchronous vibration component is considered as in Eq. (1), the corresponding error of frequency, amplitude and phase of single sinusoidal signal can be estimated by [3]

$$f_e = \min(|k\Delta f - f|, |(k+1)\Delta f - f|), \tag{2}$$

$$A_e = A_1(W(f_e) - 1), \tag{3}$$

$$\alpha_e = \frac{\pi f_e}{\Delta f}, \tag{4}$$

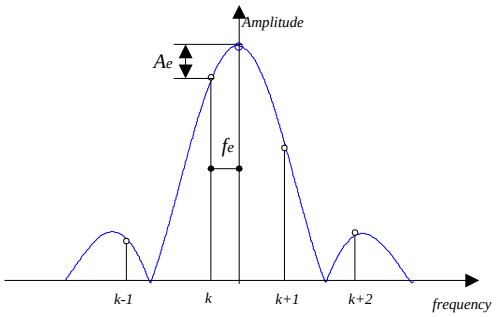

Fig. 1. Errors in frequency and amplitude by normal FFT.

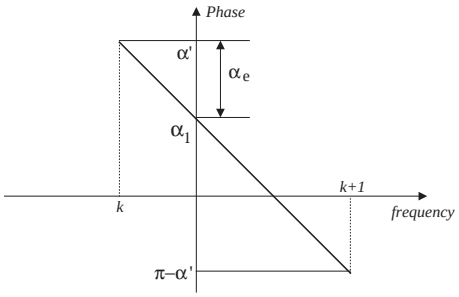

Fig. 2. Error in phase by normal FFT.

where f_e, A_e, α_e are the frequency, amplitude and phase errors, respectively. $W(f)$ is the Fourier transform of the any window function used.

It is obvious that the error of calculated frequency, amplitude and phase of sinusoidal signal can be large. Therefore, a new high-resolution spectrum based on a dichotomy searching is introduced to estimate the precise frequency, amplitude and phase of the sinusoidal signal as below.

Given N sample points of the signal, $x(0)$, $x(1)$, …, $x(N-1)$, the discrete Fourier spectrum can be calculated by

$$X(k) = \frac{1}{N}\sum_{n=0}^{N-1} x(n)\mathrm{e}^{-\mathrm{j}2\pi nk/N}. \tag{5}$$

In the above equation, suppose k has a continuous value between 0 and half of sample frequency, and the frequency interval Δf is arbitrarily small, the discrete spectrum lines should change into a continuous spectrum. Accordingly, Eq. (5) can be rewritten as

$$X(f) = \frac{1}{N}\sum_{n=0}^{N-1} x(n)\mathrm{e}^{-\mathrm{j}2\pi nf/f_s}. \tag{6}$$

The actual spectrum line of a sinusoidal component can be allocated to a frequency which makes $|X(f)|$ a peak value. The peak search process can be described as follows. Firstly, one can specify the frequency interval $[f_l, f_r]$ in which there exists a unique amplitude peak of sinusoidal component to search. Secondly, Eq. (6) can be employed to compute $|X(f_l)|$ and $|X(f_r)|$. Thirdly, above two values are compared and $f_0 = 0.5\ (f_l + f_r)$ is used to replace f_l or f_r, which corresponds to the smaller one between $|X(f_l)|$ and $|X(f_r)|$. Then, this process is repeated until the difference between f_r and f_l converge within a permitted error limit. Finally, actual peak value and corresponding precise amplitude, frequency and phase of a sinusoidal signal can be obtained according to the above dichotomy searching procedures in a specified interval $[f_l, f_r]$.

To verify the applicability and effectiveness of the above algorithm, 1024 data points are sampled at a rate of 2000 Hz through a simulated sinusoidal signal $x = 25\sin(2\pi 77.2t + 68\pi/180)$. At the same time, in order to prove the robustness of the algorithm under various noise interferences, the white noise with different noise-to-signal ratio (NTS) is added to the original signal. Table 1 shows the identified results in the noise circumstances with NTS ratio increased

Table 1
The estimated results from high-resolution spectrum

	Real value	HRS	HRS (5% noise)	HRS (10% noise)	HRS (15% noise)
Frequency (Hz)	77.2000	77.2018	77.2135	77.1732	77.1423
Amplitude	25.0000	24.9865	25.0211	24.9685	24.9314
Phase (deg)	68.0000	68.0093	68.0124	68.0612	68.0923

from 0% to 15%. It is obvious that the estimation error is relatively small although the noise level is rather high. Consequently, the high-resolution spectrum technique can be used to estimate more precisely frequency, amplitude and phase information of a sinusoidal vibration signal and its harmonic components.

2.3. Construction of purified shaft orbits

As is well known, a certain type of fault possesses its own features, but is sometimes obscured by some other vibration components. The aim of purification is to make the fault features dominant, excluding noise and some other interference components. Two approaches are proposed to purify the original vibration orbit of rotating machinery. The first approach is straightforward. The purified orbit is obtained by reconstructing corresponding harmonic components of two perpendicular directions in time domain. Firstly, certain harmonic components will be selected and their amplitude, phase and frequency information calculated using the high-resolution Fourier spectrum technique as described in Section 2.1. Finally, the above sinusoidal harmonic components in two perpendicular directions will be recombined to form a purified orbit diagram in the x–y domain, which is a typical complex domain and is very useful in rotating machinery diagnosis. Another approach is to purify the vibration signal at a certain frequency band, especially in the sub-harmonic region, by means of filtering to form a purified orbit. It is appropriate to extract the features of the non-white-noise-related fault. In general, the phase-locking, low pass filter can be employed to purify the non-white-noise components in the two perpendicular directions. Then, these two filtered signals can be recombined into a new orbit, which preserves the information in the specified frequency band and eliminates the interference from the harmonic or sub-harmonic components. Two approaches to construct purified vibration orbit can be summarized as a flowchart illustrated in Fig. 3.

3. Feature extraction from purified orbits

It is well known that the feature extraction plays a very important role in diagnosing the faults of machinery. The features should provide as much information as possible about the characteristics of the machine and should be independent to external factors, such as noise disturbance or the mounting positions of sensors. Traditionally, some vibration-related features, such as overall peak-to-peak, root-mean-square, the amplitude of harmonic and sub-harmonic components, are commonly extracted for evaluating the condition of a rotating machine under

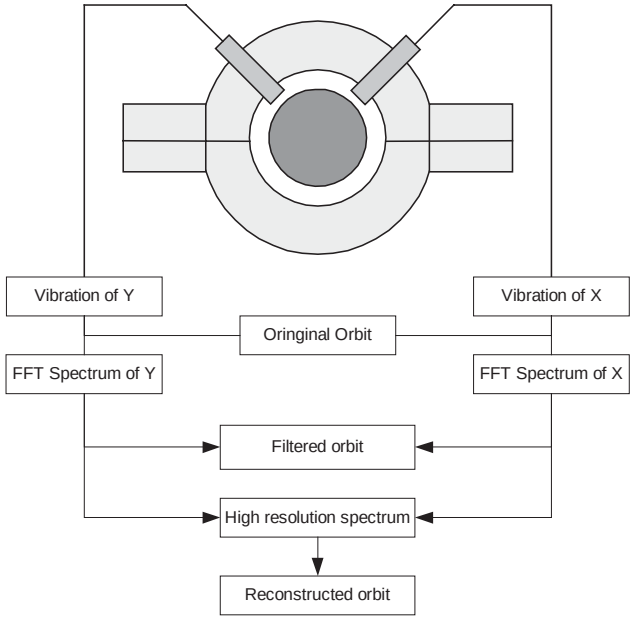

Fig. 3. The flowchart of purification and feature extraction from a vibration orbit.

operational conditions. In some circumstances, such features are sufficiently effective to monitor the condition of rotating machinery. However, since the above features cannot correlate the internal temporal and spatial features of the faults and are too sensitive to the irrelevant factors, they always fail to pinpoint the real faults in a machine. From the point of view of image processing, the purified vibration orbit can be treated as a two-dimensional image. A novel scheme is developed to extract the features from the purified orbit on the basis of image processing techniques [16] in this section. These features are very sensitive to the faults and independent to the scaling, translation and rotation of the vibration orbit.

3.1. Feature extraction from purified harmonic orbits

The purified harmonic orbit is the combination of all vibrational harmonic components in the x–y domain. Ideally, if only the effect of mass unbalance is taken into account, the orbit should be close to a circle in the x–y domain. However, the purified harmonic orbit is always complicated owing to the presence of various harmonic vibration components excited by imperfections or malfunctions. As stated in Section 2.1, the above harmonic orbit $c(t)$ can be expressed as the sum of harmonic components in the x–y domain by

$$c(t) = \sum A_n \sin(n\omega_0 t + \alpha_n) + \mathrm{j} \sum B_n \sin(n\omega_0 t + \beta_n). \tag{7}$$

where $\mathrm{j} = \sqrt{-1}$.

Furthermore, this vibration harmonic orbit can be decomposed forward (the same direction as the rotor rotation) or backward (the opposite direction to the rotor rotation) components and can

be expressed as

$$c(t) = \sum (p_n e^{jn\omega_0 t} + p_{-n} e^{-jn\omega_0 t}), \tag{8}$$

where P_n and P_{-n} indicate the amplitude of forward and backward components respectively, and can be calculated by

$$P_n = \sqrt{A_n^2 + B_n^2 + 2|A_n B_n \sin(\alpha_n - \beta_n)|}, \tag{9}$$

$$P_{-n} = \sqrt{A_n^2 + B_n^2 - 2|A_n B_n \sin(\alpha_n - \beta_n)|}. \tag{10}$$

The amplitude, frequency and phase information of harmonic vibration components can be calculated by the high-resolution spectrum technique as stated in Section 2.2. Moreover, three curve features invariant to the scaling and translation and rotation of the orbit are extracted from the purified orbit by using image processing techniques in this section.

The first curve feature F_1 is introduced to evaluate the deviation between the harmonic orbit and its synchronous forward vibration orbit and can be obtained by

$$F_1 = \frac{|p_1|}{\sum (|p_n| + |p_{-n}|)}. \tag{11}$$

If the amplitude of some other harmonic components is equal to 0 except for the synchronous forward component P_1, the orbit will be a perfect circle and $F_1 = 1$. Along with the presence of harmonic components, this index will decrease accordingly. It is obvious that this feature is independent of translation, scaling and rotation of the orbit.

The second curve feature F_2 is used to evaluate the compactivity of an orbit and can be defined as the ratio between the circumference and area of the orbit and can be calculated by

$$F_2 = \frac{S^2}{4\pi A}, \tag{12}$$

where 4π is a normalization factor to guarantee that the minimal value of F_2 is equal to 1. S is the circumference of orbit and A is the area of the orbit, which can be calculated by

$$A = \pi \sum n \left| |p_n|^2 - |p_{-n}|^2 \right|. \tag{13}$$

It is well known that a perfect circle possesses the minimal circumference in all types of orbits, which have the same area. In other words, the perfect circle is the most compact orbit and F_2 reaches its minimal value 1. Along with the presence of harmonic vibration components, the vibration orbit will become complicated and the feature F_2 will increase significantly.

In order to describe the singular behaviour due to irregular impacts caused by rubbing in the shaft orbit, the third curve feature can be introduced. Using advanced mathematics, the instantaneous curvature of an orbit can be expressed as

$$D(t) = \frac{(\dot{x}\ddot{y} - \ddot{x}\dot{y})}{(\dot{x}^2 + \dot{y}^2)^{3/2}}. \tag{14}$$

Obviously, the maximal value of instantaneous curvature F_3 can be defined as a feature to evaluate the singular characteristics in the vibration orbit, and

$$F_3 = \max(|D(t)|). \tag{15}$$

3.2. Invariant moments extracted from filtered orbits

The abnormal vibration caused by a non-white-noise-related fault, such as fluid excitation on a loose component is a typical non-stationary vibration. Using a similar method to the evaluation of the one-dimensional signal using statistical moments, two invariant moments of a two-dimensional signal will be introduced to estimate the statistical characteristic of a vibration orbit in this section.

For non-negative integers u and v, the $(u+v)th$ order moments of a vibration orbit defined on the plane $\mathbb{R}^2$ can be obtained by

$$m_{uv} = \int_c x^u y^v \, \mathrm{d}s, \tag{16}$$

where $\int_c$ denotes the integration along the orbit. The discrete form of Eq. (16) can be described as

$$m_{uv} = \sum_{j=1}^{N} \sum_{k=1}^{N} x_j^u y_k^v, \tag{17}$$

where x_j and y_k are the displacements in two orthogonal directions of the corresponding orbit. N is the number of sampling points. Furthermore, the central moments R_{uv} can be defined as

$$R_{uv} = \int_c (x - \bar{x})^u (y - \bar{y})^v \, \mathrm{d}s, \tag{18}$$

where $\bar{x} = m_{10}/m_{00}$ and $\bar{y} = m_{01}/m_{00}$. Correspondingly, the discrete central moments can be calculated by

$$R_{uv} = \sum_{j=1}^{N} \sum_{k=1}^{N} (x_j - \bar{x})^u (y_k - \bar{y})^v. \tag{19}$$

It is obvious that the central moments are invariant to the translation. In order to guarantee that the central moments are invariant to the scaling, the following normalized moments can be employed.

$$\eta_{uv} = \frac{R_{uv}}{(m_{00})^{u+v+1}}. \tag{20}$$

Finally, two moments, which are invariant to translation, scaling and rotation of the orbit, can be defined as

$$\phi_1 = \eta_{20} + \eta_{02}, \tag{21}$$

$$\phi_2 = (\eta_{20} - \eta_{02})^2 + 4\eta_{11}^2. \tag{22}$$

The moment invariant ϕ_1 is associated with the divergence of the purified orbit and is an appropriate evaluation of the presence of sub-harmonic vibration components. When the

amplitude of the sub-harmonic vibration component increases, ϕ_1 will increase correspondingly. At the same time, the moment invariant ϕ_2 is a reliable and effective evaluation of the non-symmetry in a purified orbit.

4. Diagnosing large turbines and compressors

In this section, several industrial cases are presented to show the efficiency of the purification and feature extraction approach to pinpoint the malfunctions of large industrial turbines and compressors running in oil refineries, and fertilizer and petroleum–chemical engineering plants. The vibrational displacements are collected using an eddy current proximity probe with a sensitivity 0.005 mil/mv. Each data set consists of 1024 data points and is sampled at a rate of 2000 Hz.

4.1. Harmonic vibration-related faults

Unbalance, coupling misalignment and rubbing are three typical faults associated with dominant harmonic components in the FFT spectrum of vibration. Unbalance is the most common malfunction in large rotating machinery. The rotor unbalance will cause the inertia centrifugal force, which rotates at a frequency synchronous to the shaft and transfers the rotational energy to transverse vibration. The distinctive features of unbalance are a dominant synchronous vibration component in the FFT spectrum and an almost circular orbit diagram. The coupling misalignment between two rotors is the second most common malfunction in large rotating machinery. The load produced by coupling misalignment in a specific radial direction will change twice in each revolution of the shaft. Consequently, the vibration component associated with twice the synchronous frequency becomes strong in the FFT spectrum. The rubbing between the rotor and stator of the machine is a serious malfunction that may lead to a catastrophic failure. The rubbing normally involves several physical effects, such as friction, impacting and non-linear behaviours in the rotor-bearing system. As a result, besides the synchronous vibration components, several strong harmonic components will appear in the FFT spectrum and the original shaft orbit becomes too complicated and singular.

Fig. 4 shows the original vibration orbits caused by unbalance, coupling misalignment and rubbing, respectively. Owing to the interference from noise and some other irrelevant components, it is not easy to extract the features from the original orbit. Fig. 5 shows the purified orbit based on the high-resolution spectra, which are subjected to unbalance, coupling misalignment and rubbing, respectively. After removing the noise and irrelevant components from the original orbit, three malfunctions can be clearly isolated. Additionally, the vibration amplitude of the backward orbit has increased significantly from Fig. 5 (a)–(c). Moreover, three curve features are calculated and illustrated in Table 2. Since the reconstructed orbit subjected to unbalance is nearly a circle, F_1 and F_2 are very nearly equal to 1 and F_3 is nearly equal to 0. When the coupling misalignment occurred in machinery, F_1 dropped to 0.3335 and F_2 and F_3 increased to 2.5847 and 1.0485, respectively. Finally, if rubbing exists between the stator and rotor, the purified orbit is complicated with several singular points due to the impacting effect and F_2 and F_3 increase dramatically. Moreover, to discover the accurate angular position of malfunction, the

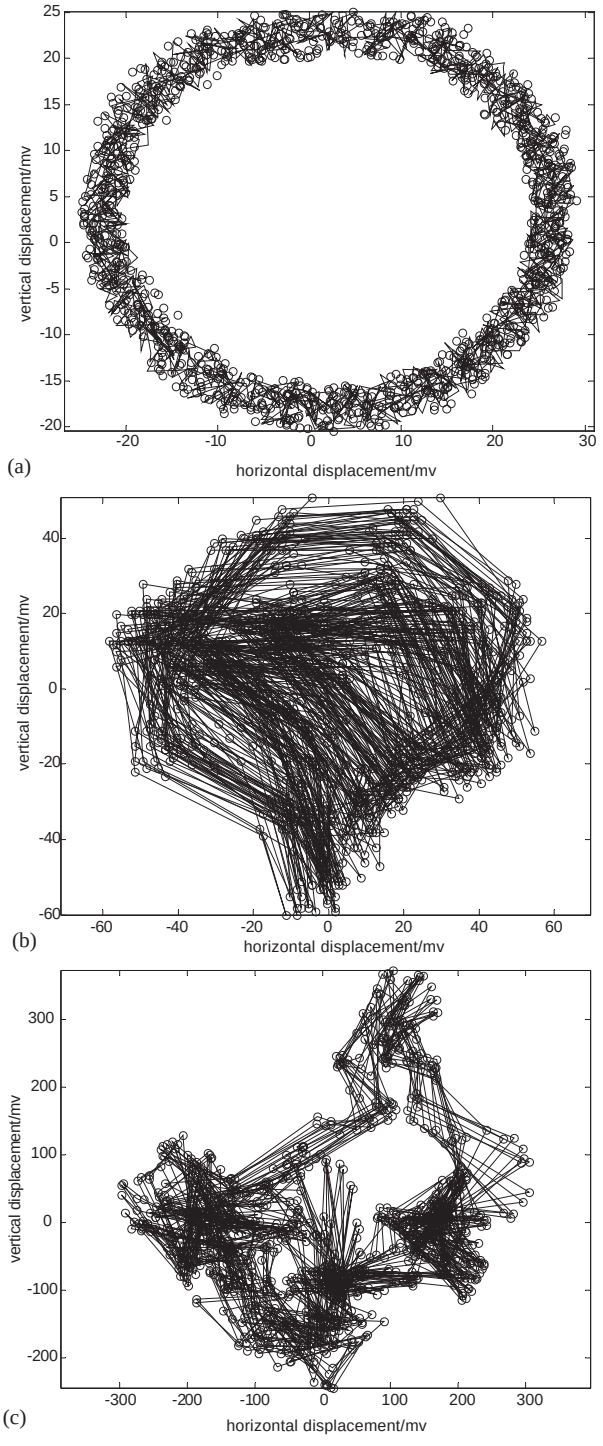

Fig. 4. Original vibration orbits with harmonic components caused by (a) unbalance, (b) coupling misalignment, (c) rubbing.

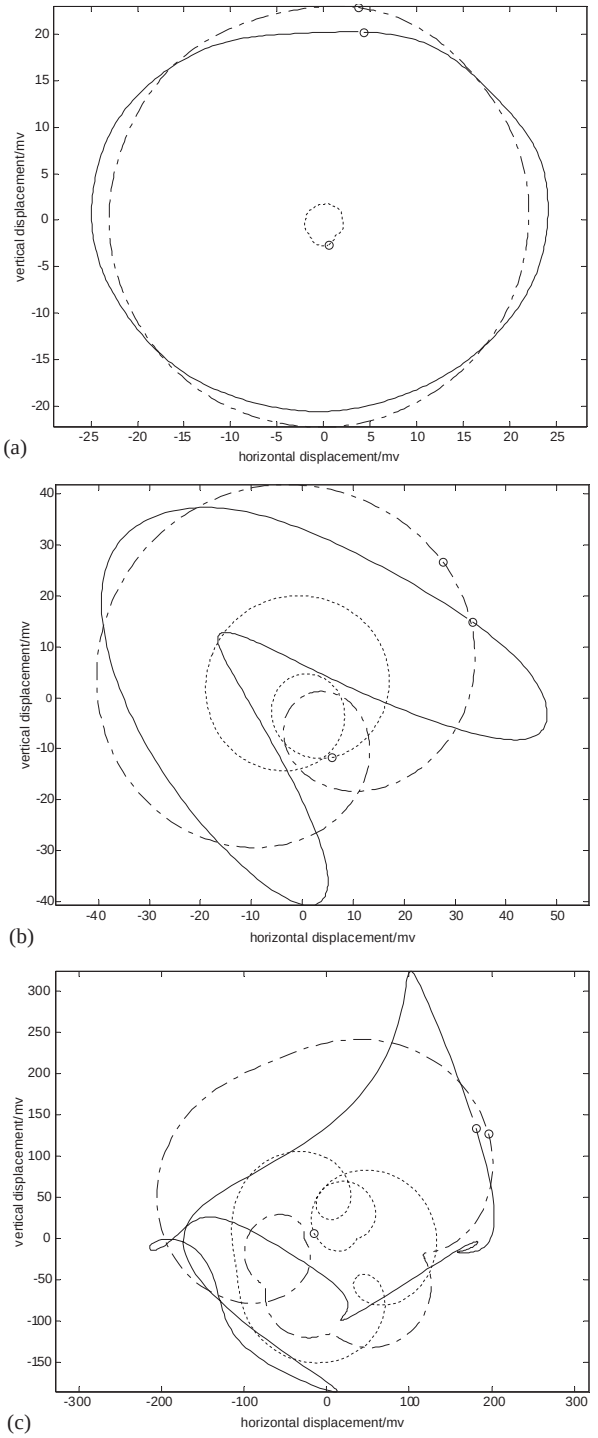

Fig. 5. Purified, forward and backward orbits with harmonic components caused by (a) unbalance, (b) coupling misalignment, (c) rubbing, —, real orbit; - -, backward orbit; -··-, forward orbit.

Table 2
The curve features with different types of malfunctions

	Unbalance	Misalignment	Rubbing
F_1	0.8559	0.3335	0.2825
F_2	1.0075	2.5847	15.1334
F_3	0.0832	1.0485	33.0587

instantaneous curvatures with three different faults are plotted in Fig. 6 (a)–(c), respectively. The maximum singular points can be detected to specify the orientation of coupling misalignment or angular position of the rubbing points.

4.2. Sub-harmonic and non-white noise-related faults

Seal wear, fluid excitation, loose components and rotating stall are four typical faults which result in dominant sub-harmonic components or non-white noise in the vibration spectrum. Fig. 7 shows the original vibration orbits when the above four malfunctions occur in the rotating machinery. Owing to the interference from synchronous and its harmonic components, the vibration features of above malfunction are almost concealed. After removing the synchronous and its harmonic components through the high-resolution spectrum and filter, the purified orbits can be obtained and shown in Fig. 8. The corresponding invariant moments can be calculated by Eqs. (21) and (22) and illustrated in Table 3. Fig. 8(a) shows the purified orbit of a rotor with the loose component when it passes through its critical speed. Since the vibration related to the loose component is excited by boundary friction force and centrifugal force, the instantaneous centre of gravity of the orbit fluctuates from time to time. Consequently, the value of the non-symmetrical feature ϕ_2 and divergence feature ϕ_1 are both extremely high. Fig. 8(b) shows the filtered orbit of a centrifugal compressor subjected to abnormal fluid excitation, which stimulates a rotor shaft vibrating abnormally once in a while. However, the instantaneous centre of gravity is stable. The non-symmetrical feature ϕ_2 and divergence feature ϕ_1 of the fluid excitation are both lower than the features associated with a loose component. Fig. 8(c) shows the reconstructed orbit of a compressor subjected to some seal wear. The orbit is distinguished by its thread ball configuration due to the presence of sub-harmonic components stimulated by friction between seal and rotor. The non-symmetrical feature ϕ_2 and divergence feature ϕ_1 of the seal wear are both lower than the features associated with the fluid excitation. Fig. 8(d) shows the reconstructed orbit of a carbon dioxide compressor subjected to rotating stall due to the mismatched operation parameters. The divergence feature ϕ_1 of rotating stall is similar to the fluid excitation, but its non-symmetrical feature ϕ_2 has dropped significantly.

In order to judge at what speed the component of the compressor began to loosen (as in the case stated above) the original orbits at different speeds in run-up stage are presented in Fig. 9. However, it is very difficult to specify what has happened in this compressor from the original vibration orbit due to the interference from some other components, especially the synchronous vibration component. However, if the filtered orbits with different speeds can be purified during the run-up of the compressor, one can determine what is happening in the compressor in the run-up stage. Two invariant moments are further calculated with different speeds during starting and

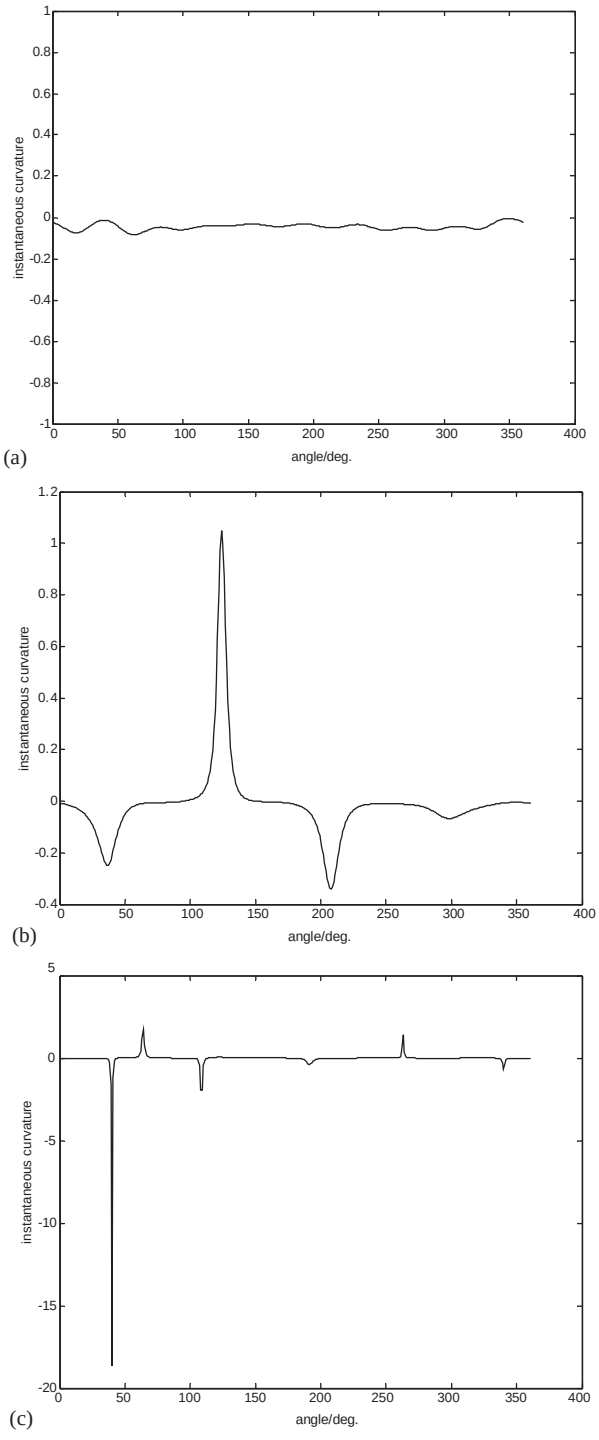

Fig. 6. The instantaneous curvature of purified orbit with harmonic components caused by (a) unbalance, (b) coupling misalignment, (c) rubbing.

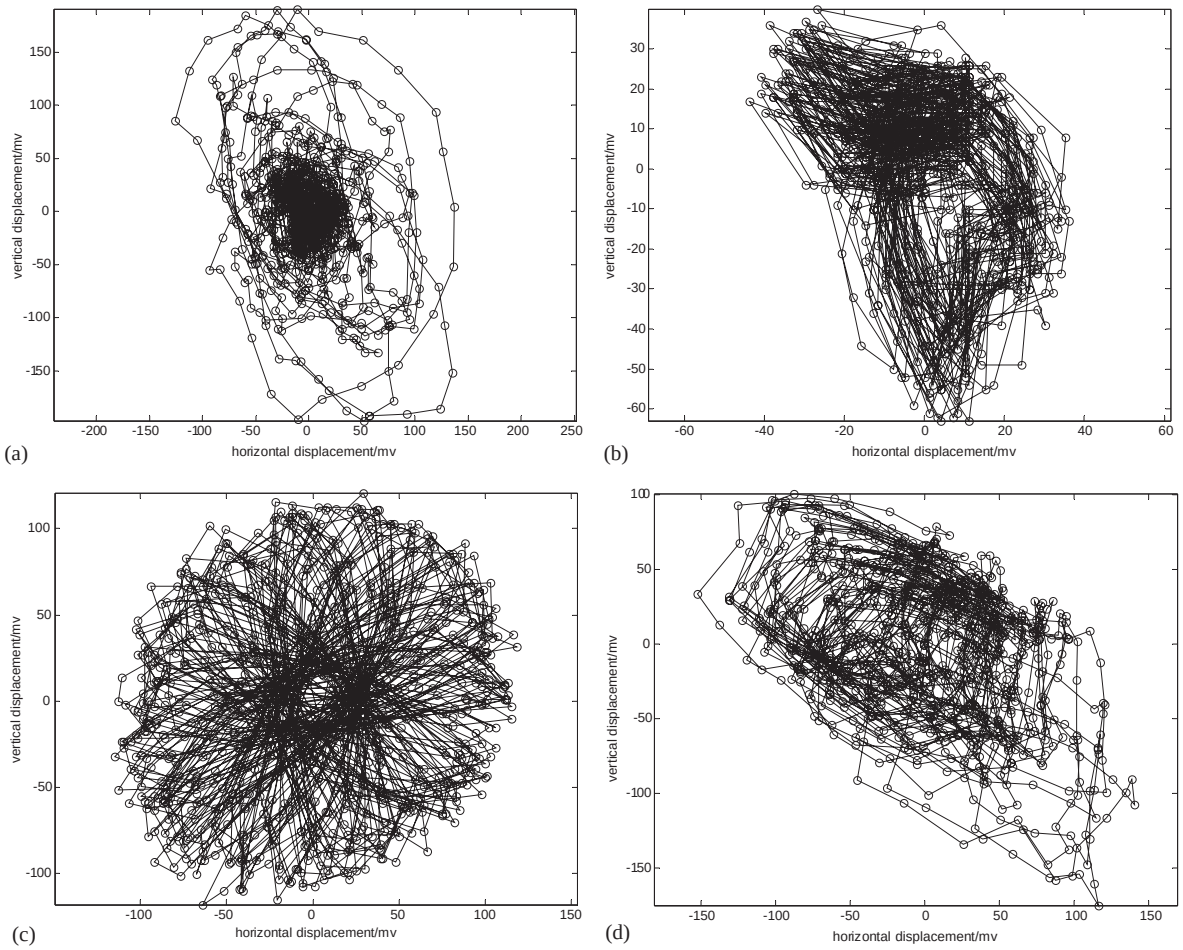

Fig. 7. Original orbits with sub-harmonic component or non-white noise caused by (a) fluid excitation, (b) seal wear, (c) rotating stall, and (d) part loosening.

are illustrated in Fig. 10. It is obvious that the above two features increase dramatically above the speed of 4827 rpm. Consequently, the operator supposed that some part must have been loosened near this speed. The compressor was then stopped for inspection and the bearing cap was found to be loose due to insufficient tightening in the latest overhaul. The compressor operated smoothly again without any abnormal vibration after this maintenance.

Moreover, to show the robust performance of invariant moments and curve features, another 10 test samples are acquired and analyzed for each type of fault. The statistical means and standard deviations of features are calculated and shown in Tables 4 and 5, respectively. Table 4 shows that three curve features will vary with the increase of harmonic vibration components from rotor unbalance to rubbing. Obviously, since three features provide an accurate quantitative evaluation of harmonic components, three faults are located at completely different regions and there is no overlap between them in the three-dimensional feature domain.

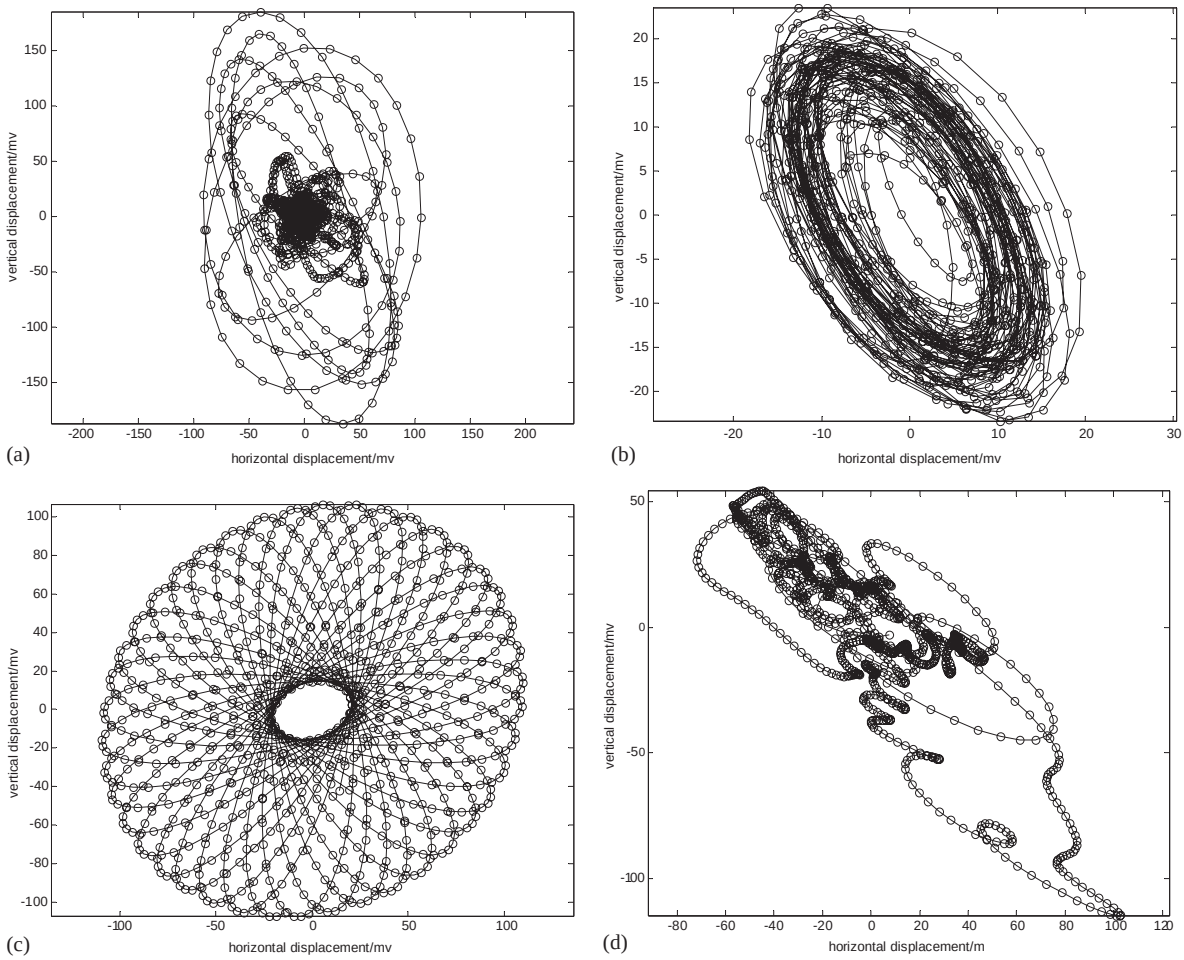

Fig. 8. Purified orbits with sub-harmonic components or non-white noise caused by (a) fluid excitation, (b) seal wear, (c) rotating stall, and (d) part loosening.

Table 3
The invariant moments with different types of malfunctions

	Fluid excitation	Loose part	Seal wear	Rotating stall
ϕ_1	5.1866	46.801	0.9201	6.3629
ϕ_2	7.5685	1513.5	0.3165	0.7338

Furthermore, Table 5 shows that four sub-harmonic or non-white noise-related faults can be isolated completely using two invariant moments. Obviously, since the two features caused by loose components are both extremely high, it is separated far from three other faults in the two-dimensional feature domain. On the other hand, the two features caused by seal wear are both the smallest, and it is not difficult to separate it from others. It is rather difficult to separate between

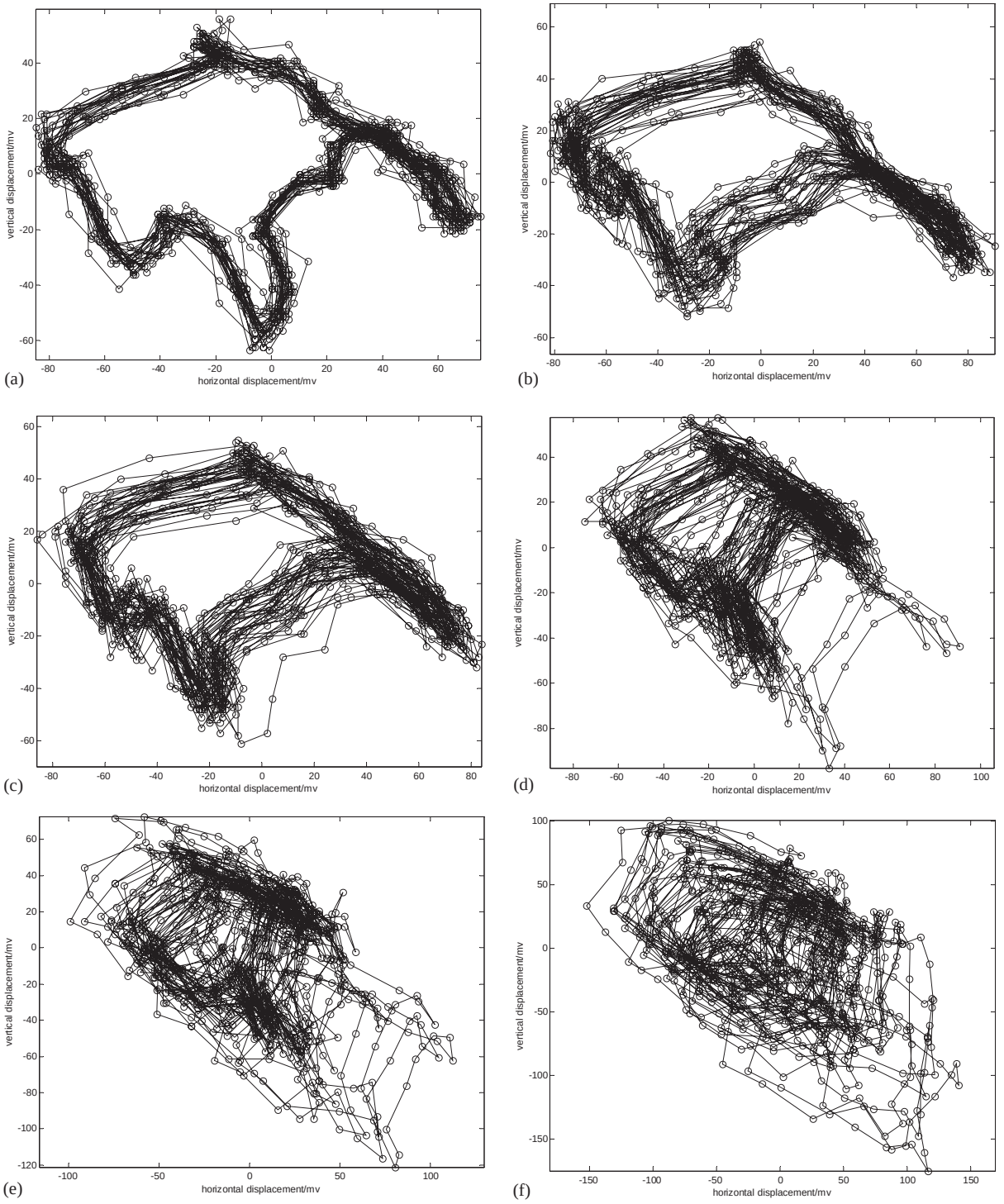

Fig. 9. The original vibration orbit of a compressor at different speed: (a) 2924 rpm, (b) 4294 rpm, (c) 4827 rpm, (d) 5872 rpm, (e) 6147 rpm, and (f) 7164 rpm.

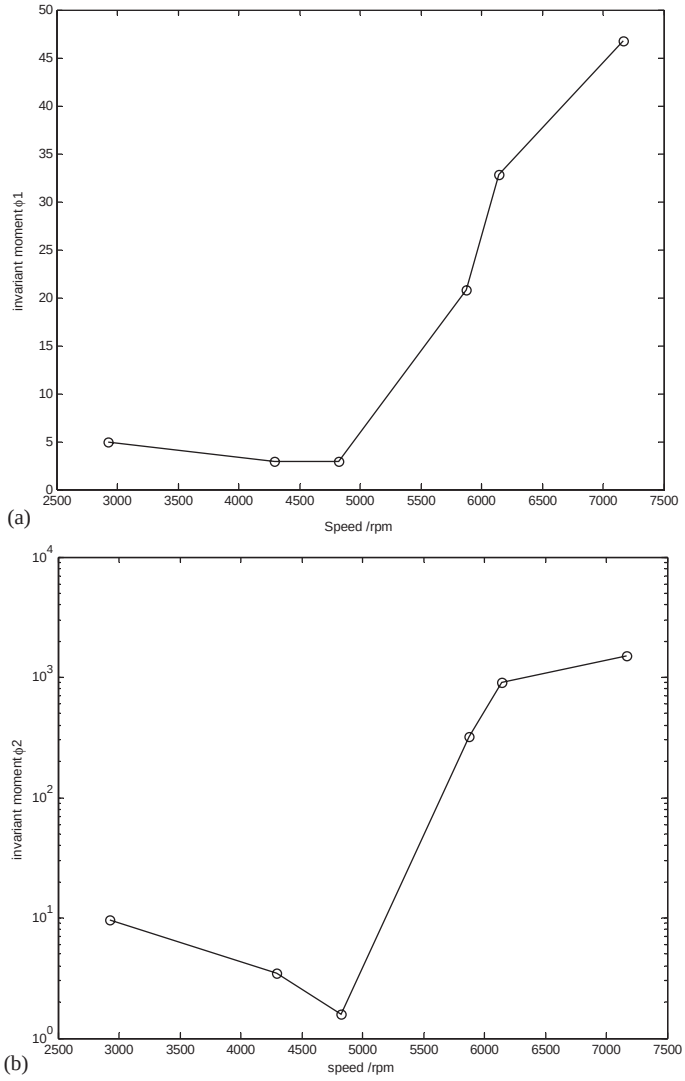

Fig. 10. Two invariant moment variations in a run-up stage: (a) divergence ϕ_1 and, (b) non-symmetrical feature ϕ_2.

Table 4
The statistical means ($\bar{F}_i$) and deviations (ΔF_i) of curve features associated different malfunctions

	Rotor unbalance		Coupling misalignment		Rubbing	
	$\bar{F}_i$	ΔF_i	$\bar{F}_i$	ΔF_i	$\bar{F}_i$	ΔF_i
$i=1$	0.8130	0.1262	0.4133	0.1272	0.2314	0.0912
$i=2$	1.0103	0.0921	3.1621	1.1231	12.212	4.1281
$i=3$	0.0622	0.0287	2.0712	1.3275	30.9432	9.2481

Table 5
The statistical means ($\bar{\phi}_i$) and deviations ($\Delta\phi_i$) of invariant moments associated different malfunctions

	Fluid excitation		Loose part		Seal wear		Rotating stall	
	$\bar{\phi}_i$	$\Delta\phi_i$	ϕ_i	$\Delta\phi_i$	$\bar{\phi}_i$	$\Delta\phi_i$	$\bar{\phi}_i$	$\Delta\phi_i$
$i=1$	5.4032	1.3198	38.120	10.281	0.8323	0.1524	8.1317	2.3113
$i=2$	8.1867	1.9084	1178.3	431.22	0.3632	0.1853	0.81234	0.2343

rotating stall and fluid excitation in practice. Fortunately, due to the inherent isotropic characteristics of rotating stall, its non-symmetrical feature ϕ_2 is lower than fluid excitation as shown in Table 5. Consequently, the invariant moments and curve features are proved highly effective and robust for pinpointing the faults in large rotating machinery.

5. Conclusions

A novel approach using vibration orbit purification and feature extraction procedures is introduced for diagnosing malfunctions in large rotating machinery. Firstly, a technique based on a high-resolution spectrum technique and multi-sensor fusion to purify the original vibration orbit of vibration is presented. The purified orbit can be reconstructed to retain the effects of malfunction-related components after removing the noise and interference. Secondly, the invariant moments and curve feature are introduced to extract the features of malfunctions which occurred in the rotating machinery. These features possess obvious significance and can be employed to quantify the vibration behaviour as well as to pinpoint the details of malfunctions in the rotor, bearing support or coupling. This new methodology is shown to be very effective and robust in diagnosing various types of malfunctions in large gas turbines and compressors under operating conditions as well as in the run-up stages. Further investigation is worthwhile in order to construct an automated intelligent diagnosis system for rotating machinery using the proposed quantitative features.

Acknowledgements

The authors are grateful to the editor and anonymous referees for valuable comments. The experimental support from Shijiazhuang Petroleum Plant, Xingjiang Petroleum-Chemical Plant and ZhenHai Oil Refinery, and financial sponsorship of National Science Foundation Council (No.50205012) and Aeronautics Foundation (No.02I52067) are gratefully acknowledged.

References

[1] J. Mathew, Monitoring the vibrations of rotating machine elements-an overview, *The Bulletin of CMCM Monash* 1 (1) (1989) 1–11.
[2] M.J. Nelson, *The Tribology Handbook*, Butterworth-Heinemann, London, 1995.

[3] D.F. Shi, Study on Holodiagnosis for large rotating machinery, Doctoral Thesis, Xian Jiaotong University, 1998.
[4] E. Downham, Vibration in rotating machinery: malfunction diagnosis—art and science, *Proceeding of the Institution of Mechanical Engineering—Vibration in Rotating Machinery*, London, UK, 1976, pp. 1–6.
[5] A. Muszynska, Improvements in lightly loaded Rotor/Bearing and Rotor/Seal Models, *American Society of Mechanical Engineers Transactions on Vibration Acoustics Stress and Reliability in Design* 110 (2) (1988) 129–136.
[6] A. Muszynska, Vibrational diagnostics of rotating machinery malfunctions, *International Journal of Rotating Machinery* 1 (3–4) (1995) 237–266.
[7] G.T. Zheng, W.J. Wang, A new cepstral analysis procedure of recovering excitations for transient components of vibration signals and applications to rotating machinery condition monitoring, *American Society of Mechanical Engineers Transactions on Journal of Vibration and Acoustics* 123 (2001) 222–229.
[8] G.T. Zheng, Vibration of a rotor system with a switching crack and detection of the crack, *American Society of Mechanical Engineers Transactions on Journal of Engineering for Gas Turbines and Power* 120 (1) (1998) 149–154.
[9] Qingfeng Meng, Liangsheng Qu, Rotating machinery faults diagnosis using Wigner distribution, *Mechanical System and Signal Processing*, 5(3) (1992) 155–166.
[10] D.F. Shi, F. Tsung, P.J. Unsworth, Adaptive time-frequency decomposition for transient vibration monitoring of rotating machinery, *Mechanical Systems and Signal Processing* 18 (2004) 127–141.
[11] Z.X. Geng, L.S. Qu, Vibrational diagnosis of machinery parts using wavelet packet techniques, *British Journal of Non-Destructive Testing* 36 (1) (1994) 11–15.
[12] L.S. Qu, Y.D. Shen, Orbit complexity: a new criterion for evaluating the dynamic quality of rotor system, *Proceedings of the Institution of Mechanical Engineers Part C* 207 (1993) 325–334.
[13] Z. Peng, Z. He, Z. Chen, F. Chu, Identification of the shaft orbit for rotating machines using wavelet modulus maxima, *Mechanical Systems and Signal Processing* 16 (4) (2002) 623–635.
[14] R.C. Lou, M.G. Kay, Multi-sensor integration and fusion in intelligent systems, *IEEE Transactions on Systems, Man and Cybernetics* 19 (5) (1989) 901–931.
[15] R.W. Ramirez, *The FFT: Fundamentals and Concepts*, Prentice-Hall, London, 1985.
[16] J. Wood, Invariant pattern recognition-review, *Pattern Recognition* 29 (1) (1996) 1–17.